Distributions and stoichiometry of dissolved nitrogen and phosphorus in the iron fertilized region near Kerguelen (Southern Ocean).

S. Blain[1,2], J. Capparos[1,2], A. Guéneuguès I. [1,2] Obernosterer[1,2], and L. Oriol[1,2]

[1]Sorbonne Universités, UPMC Univ Paris 06, UMR7621, Laboratoire d'Océanographie Microbienne, Observatoire Océanologique, 66650 Banyuls/mer, France

[2]CNRS, UMR7621, Laboratoire d'Océanographie Microbienne, Observatoire Océanologique, 66650 Banyuls/mer, France

Abstract

During KEOPS2 (Kerguelen Ocean and Plateau Compared Study 2), we determined dissolved inorganic and organic nitrogen and phosphorus species in the naturally fertilized region of Kerguelen Island (Southern Ocean,). Above 150m, stations were clearly separated by the Polar Front (PF), with concentrations of NO_3^-, NO_2^- and PO_4^{3-} overall lower north than south of the PF. Though less pronounced, a similar trend was detectable for dissolved organic nitrogen (DON) and phosphorus (DOP). At all stations offshore and above the plateau, a subsurface maximum of NH_4^+ was observed between 50 and 150 m. We examined nutrient stoichiometry by calculating the linear combination $N^* = [NO_3^-]-16\ [PO_4^{3-}]$. The majority of stations and depths revealed N* close to -3 μM, however, for surface waters north of the PF N* increased up to 6 μM. This suggests a preferential uptake of PO_4^{3-} versus NO_3^- by fast growing diatoms. Using the tracer TN_{xs} = [TDN]-16[TDP] revealed that the dissolved organic fraction significantly contributed to changes in TN_{xs}. TN_{xs} were negative for most stations and depths, and relatively constant in the layer 0-500m. As for N*, the stations north

of the PF had higher TN_{xs} in the layer 0-100m. We discuss this stoichiometric anomaly with respect to possible external sources and sinks of N and P. Additional data collected in February 2013 at two sites revealed the occurrence of a subsurface minimum of N* located just below the pycnocline that denotes a layer where remineralization of particulate organic matter with low N:P ratio P, possibly associated with preferential remineralisation of P versus N, persists throughout the season.

1. Introduction.

The first scientific expeditions in the Southern Ocean discovered high concentrations of major nutrients such as nitrate (NO_3^-) and phosphate (PO_4^{3-}) in surface waters south of 50°S (Hart, 1942). The general meridional overturning circulation that brings deep water to the surface at the southern limits of the Antarctic circumpolar current (Marshall and Speer, 2012) is the major mechanism supplying surface waters with NO_3^- and PO_4^{3-}. Most of the nutrient-rich upwelled waters are transported northward and they leave the surface north of the polar front, through their transformation into intermediate and mode waters. Despite the several months long northward transport during which the NO_3^- and PO_4^{3-} rich waters are exposed to sunlight, little phytoplankton biomass develops. This system was characterized as "high nitrate low chlorophyll" (HNLC). The major consequence of the HNLC status of the Southern Ocean is that large amounts of unused nutrients are transported back into the ocean interior where they feed the main thermocline and finally supply low and mid latitude surface waters with essential nutrients (Sarmiento et al., 2004). Another consequence is that similarly to NO_3^- and PO_4^{3-}, large amounts of upwelled dissolved inorganic carbon (DIC) are not converted to particulate organic carbon (POC) and remain in contact with the atmosphere for time periods long enough to degas carbon dioxide (CO_2) with important consequences on climate (Sigman and Boyle, 2000).

The iron hypothesis (Martin and Fitzwater, 1988) was a major advancement for our understanding of the HNLC paradox. More than two decades of intense research have confirmed that increasing iron supply stimulates primary production, major nutrient utilization and the air-to-sea flux of CO_2 in surface waters. Nutrient utilization in surface waters is therefore a diagnostic of the efficiency of the biological pump of CO_2. Nitrate utilization has also received much attention in paleoceanographic studies, because it can be inferred from the isotopic composition of N in bulk material or specific compounds of fossil organisms preserved in the sediment. Recent results provide support to the enhanced NO_3^- utilization related to higher dust deposition during the ice ages in the sub Antarctic region (Martinez-Garcia et al., 2014).

Early modelling studies on the iron hypothesis were conducted using models that did not explicitly represented the iron cycle. The effect of iron fertilization was mimicked using the extreme assumption that iron fertilization results in the complete depletion of N or P in surface waters (Gnanadesikan et al., 2003). However, this was never observed during artificial iron fertilization (Boyd et al., 2007), iron addition during deck incubations (Moore et al., 2007) or in naturally iron fertilized regions (Blain et al., 2007). For most previous research in this context, it was assumed that NO_3^- and PO_4^{3-} behave in a similar way. This is only true at first order because interesting differences were noticed (Jenkins et al., 1984; Minas and Minas, 1992; Lourey and Trull, 2001). Weber and Deutsch (Weber and Deutsch, 2010) used zonal mean distributions of NO_3^- and PO_4^{3-} in the Southern Ocean to reveal that the differential utilization of both nutrients is likely related to the composition of the phytoplankton community. Detailed investigations of blooms in varying regions of the Southern Ocean confirm different utilization of NO_3^- and PO_4^{3-} depending on the dominant species in the phytoplankton community (Arrigo, 1999; De Baar et al., 1997; Moore et al., 2007). In addition, the possible role of DOP and DON for N and P decoupling has not been

investigated, although modeling studies suggest that these organic forms may significantly contribute to the cycling of N and P in the Southern Ocean (Wang et al., 2003).

Our work presents new data on dissolved inorganic and organic nitrogen and phosphorus concentrations from the iron-fertilized regions near the Kerguelen archipelago. We present their spatial and temporal distributions, and we also discuss the stoichiometry of both nutrients.

2. Material and methods

2.1 Sampling

During KEOPS2, the samples were collected at the stations presented on the map in Fig.1. The coordinates and date of sampling are summarized in suppl table 1. Additional samples were collected during the cruise KEOPSMOOR in February 2013 at stations A3 and at station TNS-6 (suppl table 1). The samples for dissolved nitrogen and phosphorus analyses were collected with 22 12 liter Niskin bottles mounted on a rosette equipped with a Seabird SBE911-plus CTD unit. In this work, we used potential temperature (θ) and density anomaly (σ) to characterize the hydrology of the stations. A more complete description of the hydrology and the circulation is presented in (Park et al., 2014).

For NO_3^-, PO_4^{3-} and nitrite (NO_2^-), syringes (50 mL) were directly connected to the spigot of the Niskin bottles. The samples were drawn through a 0.45 µm Up-tidisc adapted to the syringe. Duplicate samples were collected. The second sample (25 mL) was poisoned with mercuric chloride ($HgCl_2$, 20 mg L^{-1}, final concentration) and stored in the dark at room temperature for later analysis. .

For ammonium (NH_4^+), samples were collected from Niskin bottles in two 50 mL Schott glass bottles. Following rinsing, the bottles were filled with 40 mL of seawater and closed

immediately to avoid contamination by air. Back in the aboard laboratory the oxidative reagent (Holmes et al., 1999) was added.

For dissolved organic nitrogen (DON) and phosphorus (DOP) analysis the samples were collected from Niskin bottles in 100 mL Schott glass bottles. The Schott glass bottles were rinsed with HCl (10%) and several times with ultrapure water between casts. The samples were then filtered through 2 combusted GF/F filters. 20 mL of the filtered samples were transferred to 20 mL PTFE vials and poisoned with 100 µl of $HgCl_2$ (4 g L^{-1}, working solution) before storage at 4°C. All analyses were performed aboard as described below.

2.2 Analytical methods

For NO_3^-, NO_2^-, PO_4^{3-}, one sample was immediately analyzed aboard with a segmented flow analyzer (Skalar) equipped with colorimetric detection using methods described in (Aminot and Kérouel, 2007). The accuracy of the methods was assessed using reference material (Certipur, Merck). The precision was in the range 1-4 %, and the limit of detection was 0.02 µM for $NO_3^-$and NO_2^-, 0.03 µM for PO_4^{3-}.

Samples for DON and DOP determination were spiked with 2.5 mL of the oxidative reagent (boric acid + sodium hydroxide + potassium peroxodisulfate), and then heated at 120°C during 30 min. After cooling, the concentrations of NO_3^- and PO_4^{3-} were determined as mentioned above. This provides the concentrations of Total Dissolved Nitrogen (TDN) and Total Dissolved Phosphorus (TDP). The concentrations of DON and DOP were calculated as follows; DON=TDN-[NO_3^-]-[NO_2^-] and DOP = TDP-[PO_4^{3-}].

Samples for NH_4^+ determination were incubated for at least 3 hours in the dark, at ambient temperature, before fluorescence measurements (λ_{exc}=370 nm λ_{emi}=460 nm) with a fluorimeter (Jabsco).

3. Results

Most of the stations are located south of the Polar Front (PF), with the exception of the coastal stations TEW-1-2 and the offshore stations TNS-1-2, TEW-7-8 and F-L that were located north of the PF (Fig.1). Station R-2, located west of the plateau had low chlorophyll concentrations in surface water throughout the season (~0.3 mg m^{-3})(Lasbleiz et al., 2014), an observation that is explained by the low iron supply (Quéroué et al. this issue). By contrast, all other stations were characterized by the development of large spring blooms consistent with higher iron supply(Lasbleiz et al., 2014). However, the development of the blooms within the iron fertilized region was not homogenous in time and space. A3-1, and stations TNS-1 to TNS-10 of the North-South transect, sampled at the beginning of the spring bloom, were characterized by low chlorophyll concentrations only slightly higher than that at station R-2. Stations TEW-1 to TEW-8 of the East-West transect, stations E-2 to E-5, and station A3-2 (second visit at station A3), were sampled a few days later, when the bloom rapidly developed with large spatial heterogeneity. The largest stocks of chlorophyll *a* within the 0-200 m layer were observed at stations F-L north of the PF and at station A3-2 above the plateau. Based on the trajectories of 2 surface drifters (Zhou et al., 2014), stations E-1, E-2, E-3, E4-E and E-5, are assumed to evolve in a quasi Lagrangian framework and their succession in time can be considered at the first order as a time series.

3.1 Two dimensional distributions of dissolved nitrogen and phosphorus.

In the upper 200m of the water column, concentrations of NO_3^- and PO_4^{3-} were $\geq$ 19 µM and $\geq$ 1 µM, respectively (Fig. 2 and 3). Concentrations were higher west of the PF (transect EW, Fig. 2) and South of the PF (transect NS, Fig. 3) and lower in surface subantarctic waters, north and east of the PF. Concentrations of NO_2^- were the highest above 150m, and below this depth NO_2^- decreased rapidly to reach values close to the limit of detection at 200m. Above 150m, NO_2^- concentrations were clearly higher at the stations in the polar front zone

(PFZ)(NO_2^- in the range 0.3-0.4 µM) than at those in the Antarctic Zone (AZ)(NO_2^- of 0.25 µM).

Along the transect EW, the highest NO_2^- concentrations were measured at TEW-1 (0.31-0.34 µM). Contrasting with the NO_2^- distribution observed along the transect NS, the stations of the AZ (i.e. west of the isocline sigma=27) had higher concentrations than those of the PFZ. NH_4^+concentrations were highest at the coastal stations. At Stations TEW-1, concentrations of NH_4^+ increased from 0.19 µM (at 10m) to 1.45 µM (close to the bottom). The same trend was observed at TEW-2 (0.17 µM at 10m and 0.39 µM close to the bottom). At all stations offshore and above the plateau, a subsurface maximum of NH_4^+ peaking at 0.5-0.6 µM was observed between 50 and 150 m. The DON distribution was characterized by a north-south gradient in the 0-150 m layer. DON concentrations above the Kerguelen plateau at Stations A3-1 and TNS-10 (6.0±1.0 µM) were similar than in the meander of the PF 6.4±1.7 µM (stations TNS-3 to TNS-7). But higher values were detectable north of the PF (8.6±1.2 µM for stations TNS-1 and TNS-2). .

For DOP, the latitudinal gradient was less pronounced, but DOP concentrations were lower above the Kerguelen plateau than at any other sites.

3.2. Speciation of dissolved nitrogen at selected sites.

3.2.1. The Kerguelen plateau station A3

The vertical distribution of different chemical nitrogen species during the two visits at station A3 are detailed in figure 4. NO_3^- distributions are discussed in more detail in the section 3.3. Concentrations of NO_2^- were, during both visits, homogeneous in the mixed layer and revealed a small maximum below the mixed layer depth (MLD). NO_2^- increased from 0.27 µM at A3-1 to 0.33 µM at A3-2 (Fig. 4b). NH_4^+ concentrations roughly doubled between the two visits (0.1 µM at A3-1 to 0.2 µM at A3-2) and clear maxima were detectable at the base

of the mixed layer. Concentrations of DON did not change between visits, however DON accounted for 20% of TDN in the mixed layer at A3-1, and this contribution increased to 25% in the upper 40 m water layer at A3-2 (data not shown). Both NO_3^- consumption and DON release during the 4 weeks that separated the two visits explained the increase in the percent DON of TDN. Below 200 m, TDN was higher at A3-1 than at A3-2. This was mainly driven by the differences in DON concentrations that were higher at A3-1 (4.7-6.7 μM) than at A3-2 (1.8-4 μM) in the 250-300 m layer (Fig. 4).

3.2.2. Stations F-S and F-L north of the Polar Front

Distinct vertical profiles of NO_2^- and NH_4^+ were observed at station F-S. Concentrations of NO_2^- decreased from 0.39 μM at 10 m to 0.22 μM at 93 m. However, we note a remarkably low value of 0.15 μM at 79 m (Fig. 5a). The NH_4^+ profile presented the same anomaly, resulting in two subsurface maxima. This feature contrasts with most other stations where a single subsurface maximum was observed, as for example at station F-L (Fig. 5b) located a few nautical miles away from F-S. We suggest that this anomaly is due to the position of F-S within the polar front where a complex mixing event at small scale could have occurred. The contribution of DON to TDN at F-S decreased continuously from 34% at 20 m to 9% at 120 m. However, close to the surface the contribution of DON was only 17% (Fig. 5d).

3.2.3. The HNLC station R-2

The vertical distribution of NO_3^- and DON revealed small variations between the surface and 200 m (Fig. 6a). DON accounted for 19% to 24% of TDN, representing intermediate values as compared to the range observed in the fertilized region. Concentrations of NO_2^- and NH_4^+ presented similar vertical distributions, decreasing rapidly below the mixed layer (Fig. 6b). Concentrations of NH_4^+ in the mixed layer (0.07 μM) were at least two fold lower than at any other stations, and NO_2^- concentrations in the mixed layer (0.3 μM) were similar to those of the mixed layers in the fertilized regions.

3.2.4. Lagrangian sites E

All stations were characterized by similar vertical distributions of NO_2^- and NH_4^+. Concentrations in the mixed layer were in the range 0.25-0.3 µM decreasing to 0.02-0.03 µM below 200 m. The vertical distributions of NH_4^+ are characterized by a subsurface maximum with concentrations (0.4-0.65 µM) two fold higher than at the surface (0.2-0.3µM). NO_3^- distributions are described in more detail in the next section. The contribution of DON to TDN in the mixed layer was in the range 15-25%. No clear temporal evolution was detectable.

3.3. Temporal evolution of the vertical distributions of nitrate and phosphate

3.3.1. The Lagrangian sites E

The vertical profiles of NO_3^- and PO_4^{3-} concentrations in the upper 200 meters of 5 stations located in the center of a meander of the PF are presented in Fig. 7. In addition, we show data from two other cruises. Samples collected in early October 1995 during the cruise ANTARES3 (Blain et al. 2001) provide data typical of winter conditions. Samples of the KEOPSMOOR profile were collected in February 2013, representing post bloom conditions. Concentrations of NO_3^- are almost identical among visits at 150 m (mean 27.5 ± 0.8 µmol L^{-1}, Fig. 7a). Above 150 m, NO_3^- concentrations change along the season. In winter, concentrations are homogenous from surface to 150 m, resulting in a mean integrated stock of 4.22 ± 0.08 mol m^{-2}. In spring, the KEOPS2 profiles qualitatively cluster in two groups. The first cluster is composed of stations TNS-5, TNS-6, E-1, E-2 and E-3, with higher NO_3^- concentrations (mean integrated stock 0-150m of 4.10 ± 0.05 mol m^{-2}) than in the group formed by stations E4-E and E-5 (mean integrated stock 0-150m of 3.90 ± 0.04 mol m^{-2}). Finally, the lowest concentrations were measured in summer (mean integrated stock 0-150m of 3.48 mol m^{-2}).

Vertical profiles of PO_4^{3-} present similar characteristics as NO_3^-, with the exception of the winter profile (Fig. 7b). The winter profile indicates that PO_4^{3-} concentrations are homogenously mixed in the upper 150m. The concentrations seem overestimated at 150m and above. We do not think that the differences result from inter-annual variability because this would have also impacted NO_3^- concentrations. The high concentrations of PO_4^{3-} measured in winter 1995 lead to a NO_3^-:PO_4^{3-} ratio of 12.5 which is low. The overestimation of PO_4^{3-} could results from methodological issues. The ANTARES3 samples were not analyzed aboard, but a few months later in a laboratory by a different analytical protocol. The lack of certified international standards necessary for a strong quality control of the accuracy precludes rigorous comparison of sample collected in 1995 with more recent samples.

Similarly to NO_3^-, we consider the mean concentration of PO_4^{3-} at 150 m (excluding the ANTARES3 PO_4^{3-} value) to estimate a mean winter PO_4^{3-}concentration in the surface layer of 1.93 ± 0.09 µmol L^{-1}, that yields an integrated winter stock of 0.30 ± 0.02 mol m^{-2}. The integrated stock for the group of stations E-1-2-3 (0.280 ± 0.004 mol m^{-2}) was higher than for the group E-4-5 (0.274 ± 0.005 mol m^{-2}). At the end of the season the integrated PO_4^{3-} stock was 0.250 mol m^{-2}.

3.3.2. The Kerguelen plateau station A3

At Station A3, vertical profiles of changes of NO_3^- and PO_4^{3-} concentrations were observed between spring and summer (Fig. 8). Albeit the stations were sampled in November 2011 and February 2013, we consider these variations as seasonal changes. The profiles of both nutrients merge at 200 m in early spring and summer (A3-1 and A3-2). However, during the second visit at A3 (A3-2), we observed that the surface layer was mixed down to 170 m. We propose that the concentrations at 200 m are a good estimate of the winter concentrations of NO_3^- and PO_4^{3-} at this station. Thus, winter stocks (0-200m) were 6.27 and 0.43 mol m^{-2} for NO_3^- and PO_4^{3-}, respectively. At the first visit at station A3 the stocks have decreased to 5.96

244 and 0.41 mol m^{-2}. Four weeks later (A3-2) they reached 5.29 and 0.36 mol m^{-2}. Finally, in
245 February the stocks were 4.77 and 0.35 mol m^{-2}.

246 **5. Discussion.**

247 The distribution of NO_3^- and PO_4^{3-} in the world's oceans were extensively studied over the
248 past decades. A major rationale for this research is the critical role of these major nutrients for
249 phytoplankton growth and therefore marine primary production. Further, concentrations of
250 NO_3^- and PO_4^{3-} are used as tracers for biogeochemical processes in the ocean (Deutsch and
251 Weber, 2012). In the Southern Ocean, south of the subantarctic front, NO_3^- and PO_4^{3-}
252 concentrations are high. They are therefore considered as non-limiting and much less attention
253 has been paid to their distribution if compared to other nutrients such as silicic acid or
254 dissolved iron. However, the relief of iron limitation by natural or artificial fertilizations
255 offers a different perspective because NO_3^- and PO_4^{3-} should be consumed as the bloom
256 develops. This has motivated the present detailed study of dissolved N and P in the naturally
257 fertilized region of Kerguelen.

258 To explore the dynamics of NO_3^- and PO_4^{3-} we examined their stoichiometry in the
259 study region. This is commonly done by establishing the ratio $r_{N:P}=[NO_3^-]:[PO_4^{3-}]$ for
260 comparison with the Redfield ratio of 16 (Redfield et al., 1963). However, the interest of $r_{N:P}$
261 is limited because this ratio is not conserved by mixing or biological processes such as uptake
262 or remineralisation (Deutsch and Weber, 2012). We therefore calculated the linear
263 combination $N^* = [NO_3^-]-16\ [PO_4^{3-}]$, similar to the parameter first introduced by (Michaels et
264 al., 1996), but omitting the constant term required to obtain a global average of N* equal to 0.
265 N* traces the impact of processes that add or remove N and P with a stoichiometry different
266 from the Redfield ratio of 16. At almost all stations and depths, N* was close to -3 µM (Fig.
267 9a). This value agrees well with the mean N* computed for regions of the Southern Ocean

close to the PF (Weber and Deutsch, 2010). A noticeable deviation from this value was observed for a set of data where N* increased from N*=-3 μM to N*=6 μM. All data with N*>0 are for samples collected in the mixed layer north of the PF, and located in a bloom where diatoms contributed to 70 % of the carbon biomass in the euphotic layer(Lasbleiz et al., 2014).

Nutrient drawdown lower than the Redfield ratio was observed previously in the Southern Ocean. During the artificial iron fertilization experiment EIFEX, an apparent differential consumption of $\Delta(NO_3^-):\Delta(PO_4^{3-})$ of 6.4 was reported (Smetacek et al., 2012). Arrigo et al.(Arrigo, 1999) and (De Baar et al., 1997) determined a nutrient drawdown ratio in diatom blooms of 9.7 and 4.4-6.1, respectively. Near Crozet, the removal of NO_3^- versus PO_4^{3-} measured in situ and during iron addition experiments revealed that the ratio was inversely related to the proportion of diatoms of the phytoplankton community (Moore et al., 2007). All these studies confirm the impact of diatom blooms on nutrient stoichiometry in the surface layer. However, the interpretations of these observations are diverse. (De Baar et al., 1997) suggested that the preferential drawdown of PO_4^{3-} during the bloom of *Fragiliaropsis kerguelensis* in the PF could be due to the reduction of nitrate reductase activity by iron limitation or due to the dominance of *Fragiliaropsis kerguelensis* with low N:P ratios considered as a specific physiological trait. These hypotheses could not explain our observations because the stations with a nutrient drawdown anomaly were located in an iron fertilized region and the diatom community was not dominated by *Fragiliaropsis kerguelensis* but rather by *Chaetoceros (Hylochaete)* spp, *Pseudo-nitzschia* spp and *Centric* sp (Lasbleiz et al., 2014).

Thus, we interpret the positive values of N* as a result of the preferential uptake of PO_4^{3-} versus NO_3^- by fast growing diatoms. Diatoms have a mean elemental N:P stoichiometry of 10 ± 4 (Sarthou et al., 2005) that differs from the Redfield value. Indeed, the

293 elemental particulate matter composition determined at the stations with positive N* during
294 KEOPS2 (Lasbleiz et al., 2014) exhibits a mean ratio of PON:POP of 10.5± 3.3 which is
295 consistent with the observed nutrient drawdown $\Delta(NO_3^-):\Delta(PO_4^{3-})$ of 8. We suggest that the
296 preferential allocation of resources to the P-rich assembly of the cell machinery by
297 exponentially growing cells is the most likely explanation for our observations (Klausmeier et
298 al., 2004). The anomaly observed for the present data set is not linked to a particular species
299 but to general traits of the diatom community responding to iron fertilization.

300 As a variant of N* , the tracer DIN_{xs}, takes into account NO_2^- and NH_4^+ (Hansell et al.,
301 2007), but none of those tracers consider the organic pools of N and P. (Landolfi et al., 2008)
302 have defined the tracer TN_{xs} = [TDN]-16[TDP] and have shown that the dissolved organic
303 fraction significantly contributes to changes in TN_{xs}. For example, relying on N* only, can
304 lead to an underestimation of N_2 fixation at the global scale (Landolfi et al., 2008). In the case
305 of KEOPS2, the contribution of DON and DOP to TDN and TDP could reach 30%. We have
306 therefore considered TDN and TDP at all KEOPS2 stations where these measurements were
307 available (Fig. 9b). TDN=f(TDP) reveals more dispersion of the data than $NO_3^-=f(PO_4^{3-})$,
308 mainly due to the lower analytical precision for DOP and DON determinations. Still, clear
309 trends are detectable. TN_{xs} were negative for most stations and depths, and relatively constant
310 in the layer 0-500m. As for N* the stations north of the PF had higher TN_{xs} in the layer 0-
311 100m.

312 When a water parcel is considered, N* is affected by the redistribution of N and P
313 between the inorganic and the organic pools, whereas TN_{xs} is only affected by net non-
314 redfieldien sources or sinks of N and P. Consequently, the positive anomaly observed for
315 TN_{xs} in surface waters north of the PF can be explained by three possible mechanisms:
316 Deposition of N rich material from the atmosphere, N_2 fixation and export of P rich material.
317 The region of Kerguelen receives low quantities of atmospheric material (Heimburger et al.,

318 2012; Wagener et al., 2008) which is mainly from natural origin, such as desert dust, that
319 contains little nitrogen compared to phosphorus (Zamora et al., 2013). This is confirmed by
320 the low N deposition rate estimated around Crozet Island (2 nmol m^{-2} d^{-1}; Planquette et al.,
321 2007). We can therefore refute the deposition of N rich material as the cause of the TN_{xs}
322 anomaly. The second hypothesis involves N_2 fixation. To date, N_2 fixation was not reported to
323 occur in the cold waters of the Southern Ocean. However, during KEOPS2 detectable N_2
324 fixation rates were measured at different stations with a few exceptionally high values (~ 250
325 µmol m^{-2} d^{-1}) in the mixed layer of station F-L (Gonzàlez et al. this issue)). Such high fixation
326 rates could contribute to an enrichment of about 1% of TDN that is not enough to create the
327 observed anomaly. If N_2 fixation was a dominant process driving the N:P stoichiometry at this
328 station, POM elemental composition should be also affected. Generally, N_2 fixing
329 microroganisms have a high N:P ratio (Laroche, J. and Breitbarth, E., 2005). Such high ratios
330 are at odds with the low N:P measured in the POM at station F-L (Lasbleiz et al., 2014). The
331 third hypothesis for explaining the anomaly relies on the export of P rich material from the
332 mixed layer. We do not have direct measurements of N:P in the exported material, but we
333 already mentioned above that the elemental composition of particulate matter at station F-L
334 yielded the lowest N:P ratio in POM (Lasbleiz et al., 2014). This provides support that the
335 export of P rich material could result in high TN_{xs} values north of the PF. We propose that the
336 anomaly of TN_{xs} results from the imprint on stoichiometry of the diatom bloom which
337 consumed and exported phosphorus in a ratio below the Redfield value.
338 During KEOPS2 rapidly growing diatom blooms were also sampled at other stations
339 located south of the PF, but anomalies similar to those at F-L were not observed. We discuss
340 here the case of stations A3 and E-4W, which had similar chlorophyll concentrations as F-L.
341 Station A3 had a contribution of diatoms to carbon biomass and dominant diatom species
342 similar to F-L (these features are not available for E4-W) (Lasbleiz et al., 2014). There is no

343 reason that the physiological features of exponentially growing diatoms as revealed for station
344 F-L do not apply to the diatoms growing at stations A3 and E4-W. It is, however, possible
345 that the resulting effect is not large enough to translate into N* or TN_{xs} anomalies. A possible
346 explanation could be the differences in the age of the blooms. The stoichiometry would be
347 less affected in a younger bloom as compared to a bloom of longer duration. This hypothesis
348 cannot be fully verified due to the poor temporal resolution of the satellite ocean color images
349 available. Another or complementary explanation is the difference in the mixed layer depths
350 that were 50 m and 150 m at stations F-L and A3-2, respectively. Such a deep mixed layer as
351 observed at station A3-2 resulted likely from a deep episodic mixing event generated by
352 strong wind prevailing during the day preceding our visit. The deepening could have
353 dampened the anomaly by diluting and mixing the affected water parcel with underlying
354 water having a typical stoichiometry (e.g. N* or TN_{xs} around -3).

355 In February 2013, two years after the KEOPS2 cruise, we had the possibility to return to two
356 sites visited during KEOPS2 (stations A3 and TNS-6), and obtain measurements for the
357 concentrations of NO_3^- and PO_4^{3-}. These data, in combination with KEOPS2 data allowed us
358 to compare N* during two different seasons (Fig. 10). In the mixed layer, little changes of N*
359 were observed between spring and summer. However, in summer, N* exhibited a clear
360 subsurface minimum between 100-200 m, at both stations. Denitrification is a process that
361 could produce this subsurface feature. But denitrification would require low oxygen
362 concentrations that are not observed at these stations.. In a general manner, preferential
363 remineralisation of P versus N in the water column is supported by an increase of N:P in high
364 molecular dissolved organic matter (Clark, L. L. et al., 1998) in particulate matter (Copin-
365 Montegut and Copin-Montegut, 1978) and in supernatant of sediment trap material (Lourey et
366 al., 2003). The observation of the N* subsurface minimum at the end of the season, but not at
367 the beginning implies a temporal cumulative effect. The minimum is located just below the

mixed layer in the region of the pycnocline that presents the highest density gradient. This could represent a zone with a higher residence time for sinking particles resulting in an accumulation of biomass. Consequently, the remineralization would also be increased in this layer compared to the rest of the water column resulting in a higher accumulation of PO_4^{3-} relative to NO_3-. This effect might be amplified by the occurrence of particulate organic matter with low N:P ratio resulting from diatom accumulation at the pycnocline. The subsurface minimum being located above 200 m depth, it is erased when the winter mixing occurs.

To our knowledge such a subsurface minimum has not be reported in the Southern Ocean. This could be due to the limited studies that investigate concurrently dissolved N and P biogeochemistry, and due to the lack of samples collected at the appropriate vertical and temporal time scale. Our finding raises several further questions. Is the subsurface minimum of N* a particular feature of iron fertilized regions? What is the link between its occurrence and the strength of stratification of the water column? And what is the role of this layer in the remineralisation of carbon? These questions argue for future detailed investigations of the cycling of both elements in the upper layer of the Southern Ocean.

385

386 **Figure captions**

387

388 **Figure 1**: Map of the KEOPS2 study area. The locations of the stations are marked by color
389 dots. Blue indicates the stations of the North-South transect (TNS), green indicates the
390 stations of the East-West transect (TEW), orange indicates the stations E located in the
391 meander of the polar front (zoom panel). Red stands for other stations located in the fertilized
392 region and black stands for the station located in the HNLC region. Detailed positions of the
393 stations are given in supplementary Table 1.

394

395 **Figure 2**: Vertical sections of dissolved nitrogen and phosphorus species along the East-West
396 transect (TEW). (a) Nitrate, (b) Ammonium, (c) Phosphate, (d), Nitrite, (e) Dissolved organic
397 nitrogen, (f) Dissolved organic phosphorus. The isolines for sigma are plotted on each panel.

398

399 **Figure 3**: Vertical sections of dissolved nitrogen and phosphorus species along the North-
400 South transect (TNS). (a) Nitrate, (b) Ammonium), (c) Phosphate, (d), Nitrite, (e) Dissolved
401 organic nitrogen, (f) Dissolved organic phosphorus. The isolines for sigma are plotted on each
402 panel.

403

404

405 **Figure 4**: Dissolved nitrogen speciation at station A3-1 (a, b) and at station A3-2 (c, d) during
406 KEOPS2. Depth profiles of temperature and sigma are plotted on each panel.

407

408 **Figure 5:** Dissolved nitrogen speciation at stations F-L and F-S during KEOPS2.

409

410 **Figure 6:** Dissolved nitrogen speciation at station R-2.

411

412 **Figure 7** : Temporal variability of the vertical profiles of concentrations of NO_3^- (a) and
413 PO_4^{3-} (b) for stations located in the meander of the Polar Front. Details for profiles of
414 KEOPSMOOR (February 2013) and ANTARES3 (October 1995) are provided in the text.

415

416 **Figure 8**: Temporal variability of the vertical profiles of concentrations of NO_3^- (a) and PO_4^{3-}
417 (b) at the station A3.

418

419 **Figure 9**: (a) Comparison of concentrations of NO_3^- versus PO_4^{3-}. Dots denote the samples
420 and lines show different values of $N^* = NO_3^- - r_{N:P}\, PO_4^{3-}$ (b) Comparison of concentrations of
421 TDN versus TDP, Dots denote the samples and lines show different values of TNxs = TDN -
422 $r_{N:P}$ TDP .

423

424 **Figure 10**: Depth profiles of N* at stations A3 (a) and TNS-6 (b) for the month of November
425 (in red) and February (in blue). Vertical profiles of sigma are shown with the same color code.

426

427 **Acknowledgment :**
428 We thank the chief scientist Bernard Quéguiner, the captain Bernard Lassiette and crew of the
429 R/V Marion Dufresne for their support aboard. We thank C. Lo Monaco for providing us
430 with the CTD profiles of KEOPSMOOR. This work was supported by the French Research
431 program of INSU-CNRS LEFE−CYBER (Les enveloppes fluides et l'environnement –Cycles
432 biogéochimiques, environnement et ressources), the French ANR (Agence Nationale de la
433 Recherche, SIMI-6 program, ANR-10-BLAN-0614), the French CNES (Centre National
434 d'Etudes Spatiales) and the French Polar Institute IPEV (Institut Polaire Paul−Emile Victor).

435

Bibliography

Aminot, A. and Kérouel, R.: Dosage automatique des nutriments dans les eaux marines : méthodes en flux continu, Ifremer., 2007.

Arrigo, K. R.: Phytoplankton Community Structure and the Drawdown of Nutrients and CO2 in the Southern Ocean, Science, 283(5400), 365–367, doi:10.1126/science.283.5400.365, 1999.

De Baar, H. J. W., Van Leeuwe, M. A., Scharek, R., Goeyens, L., Bakker, K. M. J. and Fritsche, P.: Nutrient anomalies in Fragilariopsis kerguelensis blooms, iron deficiency and the nitrate/phosphate ratio (A. C. Redfield) of the Antarctic Ocean, Deep Sea Res. Part II Top. Stud. Oceanogr., 44(1-2), 229, 1997.

Blain, S., Quéguiner, B., Armand, L., Belviso, S., Bombled, B., Bopp, L., Bowie, A., Brunet, C., Brussaard, K., Carlotti, F., Christaki, U., Corbière, A., Durand, I., Ebersbach, F., Fuda, J. L., Garcia, N., Gerringa, L. J. A., Griffiths, F. B., Guigue, C., Guillerm, C., Jacquet, S., Jeandel, C., Laan, P., Lefèvre, D., Lomonaco, C., Malits, A., Mosseri, J., Obernosterer, I., Park, Y. H., Picheral, M., Pondaven, P., Remenyi, T., Sandroni, V., Sarthou, G., Savoye, N., Scouarnec, L., Souhault, M., Thuillers, D., Timmermans, K. R., Trull, T., Uitz, J., Van-Beek, P., Veldhuis, M. J. W., Vincent, D., Viollier, E., Vong, L. and Wagener, T.: Effect of natural iron fertilisation on carbon sequestration in the Southern Ocean, Nature, 446(7139), 1070–1075, doi:doi:10.1038/nature05700, 2007.

Boyd, P. W., Jickells, T., Law, C., Blain, S., Boyle, E. A., Buesseler, K. O., Coale, K. H., Cullen, J. J., De Baar, H. J. W., Follows, M., Harvey, M., Lancelot, C., Levasseur, M., Owens, N. J. P., Pollard, D. A., Rivkin, R. B., Sarmiento, J. L., Schoemann, V., Smetacek, V., Takeda, S., Tsuda, A., Turner, D. R. and Watson, A.: Mesoscale iron enrichment experiments 1993-2005: Synthesis and future directions, Science, 315, 612–617, doi:DOI: 10.1126/science.1131669, 2007.

Clark, L. L., Ingall, E. and Benner, R.: Marine phosphorus iselectively remineralized, Nature, 393, 426, 1998.

Copin-Montegut, C. and Copin-Montegut, G.: the chemistry of particulate matter from the south indien and antarctic ocean, Deep Sea Res., 25, 911–931, 1978.

Deutsch, C. and Weber, T.: Nutrient Ratios as a Tracer and Driver of Ocean Biogeochemistry, Annu. Rev. Mar. Sci., 4(1), 113–141, doi:10.1146/annurev-marine-120709-142821, 2012.

Gnanadesikan, A., Sarmiento, J. L. and Slater, R. D.: Effects of patchy ocean fertilization on atmospheric carbon dioxide and biological production, Glob. Biogeochem. Cycles, 17(2), doi: 10.1029/2002GB001940, 2003.

Hansell, D. A., Olson, D. B., Dentener, F. and Zamora, L. M.: Assessment of excess nitrate development in the subtropical North Atlantic, Maine Chem., 206, 562–579, 2007.

Hart, T. J.: Phytoplankton periodicity in Antarctic surface water, Discov. Rep., VIII, 1–268, 1942.

Heimburger, A., Losno, R., Triquet, S., Dulac, F. and Mahowald, N.: Direct measurements of atmospheric iron, cobalt, and aluminum-derived dust deposition at Kerguelen Islands, Glob. Biogeochem. Cycles, 26(4), GB4016, doi:10.1029/2012GB004301, 2012.

Holmes, R. M., Aminot, A., Kérouel, R., Hooker, B. and peterson, B.: a simple and precise method for measuring ammonium in marine and freshwater ecosystem, , 56(10), 1801–1808, 1999.

Jenkins, B. D., Gordon, L. I. and Nelson, D. M.: Nutrient depletion indicates high primary productoivity in the Weddel Sea, Nature, 309, 51–54, 1984.

Klausmeier, C. A., Litchman, E., Daufresne, T. and Levin, S. A.: Optimal nitrogen-to-phosphorus stoichiometry of phytoplankton, Nature, 429(6988), 171–174, doi:10.1038/nature02454, 2004.

Landolfi, A., Oschlies, A. and Sanders, R.: Organic nutrients and excess nitrogen in the North Atlantic subtropical gyre, Biogeosciences, 5(5), 1199–1213, doi:10.5194/bg-5-1199-2008, 2008.

Laroche, J. and Breitbarth, E.: Importance of the diazotrophs as a source of new nitrogen in the ocean, J. Sea Res., 53(1-2), 67–91, 2005.

Lasbleiz, M., Leblanc, K., Blain, S., Ras, J., Cornet-Barthaux, V., Hélias Nunige, S. and Quéguiner, B.: Pigments, elemental composition (C, N, P, and Si), and stoichiometry of particulate matter in the naturally iron fertilized region of Kerguelen in the Southern Ocean, Biogeosciences, 11(20), 5931–5955, doi:10.5194/bg-11-5931-2014, 2014.

Lourey, M. J., Trull, T. W. and Sigman, D. M.: Sensitivity of δ^{15} N of nitrate, surface suspended and deep sinking particulate nitrogen to seasonal nitrate depletion in the Southern Ocean, Glob. Biogeochem. Cycles, 17(3), n/a–n/a, doi:10.1029/2002GB001973, 2003.

Lourey, M. and Trull, T. W.: seasonal nutreint depletion and carbon export in the subantarctic and polar frontal zones of the Southern Ocean, J. Geophys. Res. Oceans, 106(C12), 31463–31487, 2001.

Marshall, J. and Speer, K.: Closure of the meridional overturning circulation through Southern Ocean upwelling, Nat. Geosci., 5(3), 171–180, doi:10.1038/ngeo1391, 2012.

Martinez-Garcia, A., Sigman, D. M., Ren, H., Anderson, R. F., Straub, M., Hodell, D. A., Jaccard, S. L., Eglinton, T. I. and Haug, G. H.: Iron Fertilization of the Subantarctic Ocean During the Last Ice Age, Science, 343(6177), 1347–1350, doi:10.1126/science.1246848, 2014.

Martin, J. M. and Fitzwater, S. E.: Iron deficiency limits phytoplankton growth in the north-east Pacific subarctic, Nature, 331, 341–343, 1988.

Michaels, A. F., Olson, D., Sarmiento, J., Ammerman, J. W., Fanning, K. A., Jahnke, R. A., Knap, A. H., Lipschultz, F. and Prospero, J.M.: Inputs, losses and transformations of nitrogen and phosporus in the pelagic North Atlantic Ocean, Biogeochemistry, 35, 181–226, 1996.

Minas, H. J. and Minas, M.: : Net community production in "High Nutrient-Low Chlorophyll" waters of the tropical and antarctic oceans: grazing versus iron hyopthesis, Oceanol. Acta, 15(2), 145–162, 1992.

Moore, C. M., Hickman, A. E., Poulton, A. J., Seeyave, S. and Lucas, M. I.: Iron–light interactions during the CROZet natural iron bloom and EXport experiment (CROZEX): II—Taxonomic responses and elemental stoichiometry, Deep Sea Res. Part II Top. Stud. Oceanogr., 54(18-20), 2066–2084, doi:10.1016/j.dsr2.2007.06.015, 2007.

Park, Y.-H., Durand, I., Kestenare, E., Rougier, G., Zhou, M., d' Ovidio, F., Cotté, C. and Lee, J.-H.: Polar Front around the Kerguelen Islands: An up-to-date determination and associated circulation of surface/subsurface waters, J. Geophys. Res. Oceans, doi:10.1002/2014JC010061, 2014.

Planquette, H., Statham, P. J., Fones, G., Charette, M. A., Moore, C. M., Salter, I., Nédélec, F. H., Taylor, S. L., French, M., Baker, A. R., Mahowald, N. and Jickells, T. D.: Dissolved iron in the vicinity of the Crozet islands, Southern Ocean, Deep-Sea Res. II, 54, 1999–2019, 2007.

Redfield, A. C., Ketchum, B. H. and Richards, F. A.: The influence of organism on the composition of seawater, in The Sea, Hill N. M., New York., 1963.

Sarmiento, J. L., Gruber, N., Brzezinsky, M. A. and Dunne, J. P.: High-latitude controls of thermocline nutrients and low latitude biological productivity, Nature, 427, 2004.

Sarthou, G., Timmermans, K. R., Blain, S. and Treguer, P.: Growth physiology and fate of diatoms in the ocean: a review, J. Sea Res., 53(1-2), 25, 2005.

Sigman, D. M. and Boyle, E. A.: Glacial/interglacial variations in atmospheric carbon dioxide, Science, 407, 859–869, 2000.

Smetacek, V., Klaas, C., Strass, V. H., Assmy, P., Montresor, M., Cisewski, B., Savoye, N., Webb, A., d' Ovidio, F., Arrieta, J. M., Bathmann, U., Bellerby, R., Berg, G. M., Croot, P., Gonzalez, S., Henjes, J., Herndl, G. J., Hoffmann, L. J., Leach, H., Losch, M., Mills, M. M., Neill, C., Peeken, I., Röttgers, R., Sachs, O., Sauter, E., Schmidt, M. M., Schwarz, J., Terbrüggen, A. and Wolf-Gladrow, D.: Deep carbon export from a Southern Ocean iron-fertilized diatom bloom, Nature, 487(7407), 313–319, doi:10.1038/nature11229, 2012.

Wagener, T., Guieu, C., Losno, R., Bonnet, S. and Mahowald, N.: Revisiting atmospheric dust export to the southern hemisphere ocean: biogeochemical implication, Glob. Biogeochem. Cycles, 22(GB2006), doi:10.1029/2007GB002984., 2008.

Wang, X., Matear, R. J. and Trull, T. W.: Nutrient utilization ratios in the Polar Frontal Zone in the Australian sector of the Southern Ocean: A model., Glob. Biogeochem. Cycles, 17(1), n/a–n/a, doi:10.1029/2002GB001938, 2003.

Weber, T. S. and Deutsch, C.: Ocean nutrient ratios governed by plankton biogeography, Nature, 467(7315), 550–554, doi:10.1038/nature09403, 2010.

Zamora, L. M., Prospero, J. M., Hansell, D. A. and Trapp, J. M.: Atmospheric P deposition to the subtropical North Atlantic: sources, properties, and relationship to N deposition, J. Geophys. Res. Atmospheres, 118(3), 1546–1562, doi:10.1002/jgrd.50187, 2013.

Zhou, M., Zhu, Y., d' Ovidio, F., Park, Y.-H., Durand, I., Kestenare, E., Sanial, V., Van-Beek, P., Queguiner, B., Carlotti, F. and Blain, S.: Surface currents and upwelling in Kerguelen Plateau regions, Biogeosciences Discuss., 11(5), 6845–6876, doi:10.5194/bgd-11-6845-2014, 2014.

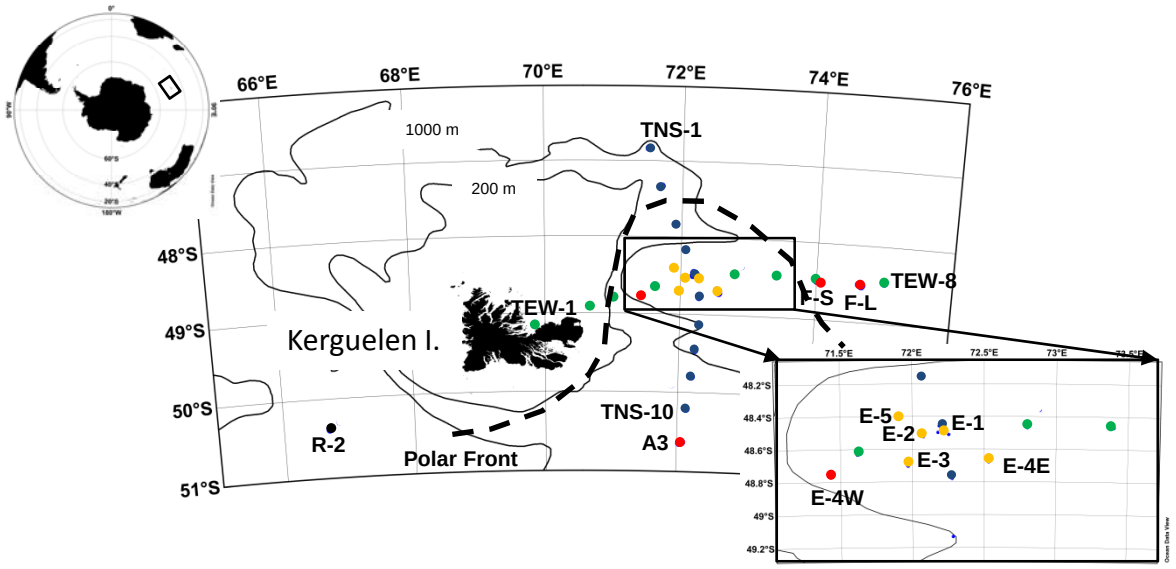
66°E
68°E
70°E
72°E
74°E
76°E
48°S
49°S
50°S
51°S
1000 m
200 m
TNS-1
TEW-1
TEW-8
F-S
F-L
Kerguelen I.
TNS-10
A3
R-2
Polar Front
71.5°E
72°E
72.5°E
73°E
48.2°S
48.4°S
48.6°S
48.8°S
49°S
49.2°S
E-5
E-2
E-1
E-3
E-4E
E-4W

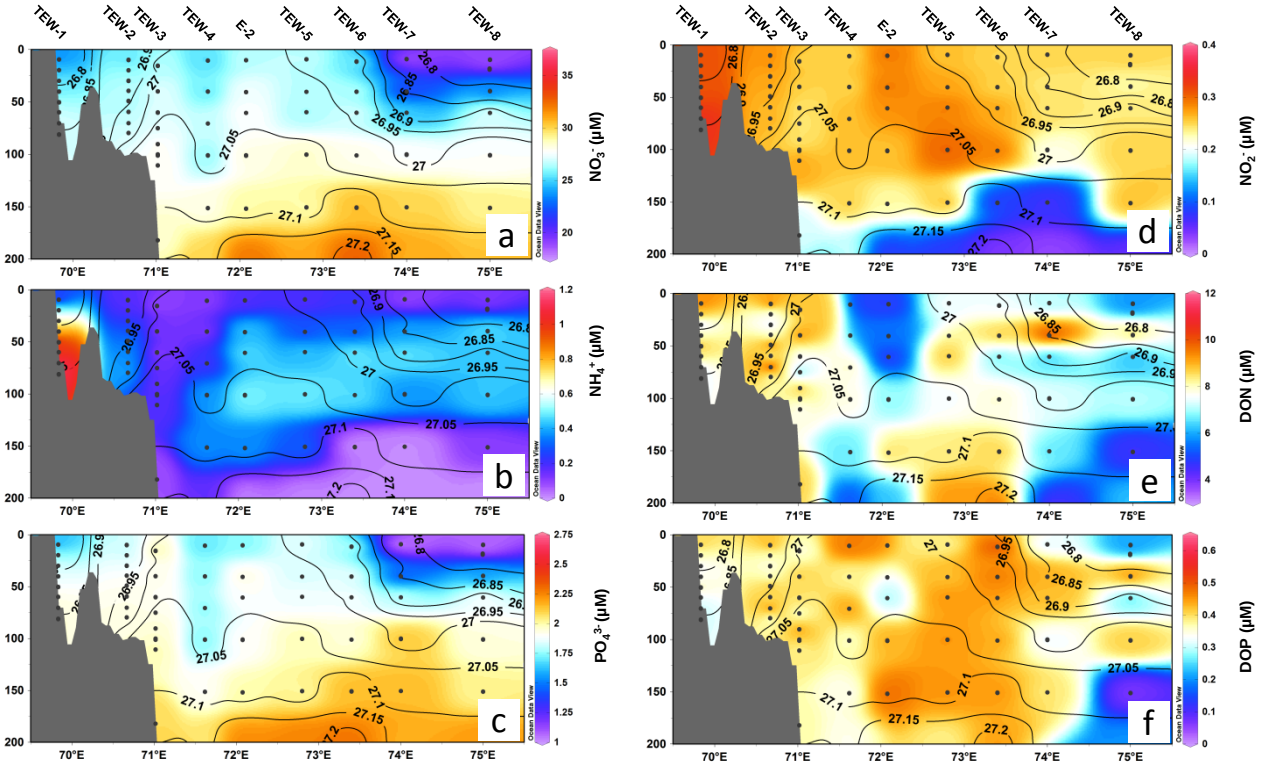
TEW-1
TEW-2
TEW-3
TEW-4
E-2
TEW-5
TEW-6
TEW-7
TEW-8
a
b
c
d
e
f
NO_3^- (µM)
NH_4^+ (µM)
PO_4^{3-} (µM)
NO_2^- (µM)
DON (µM)
DOP (µM)
70°E
71°E
72°E
73°E
74°E
75°E

Figure 2

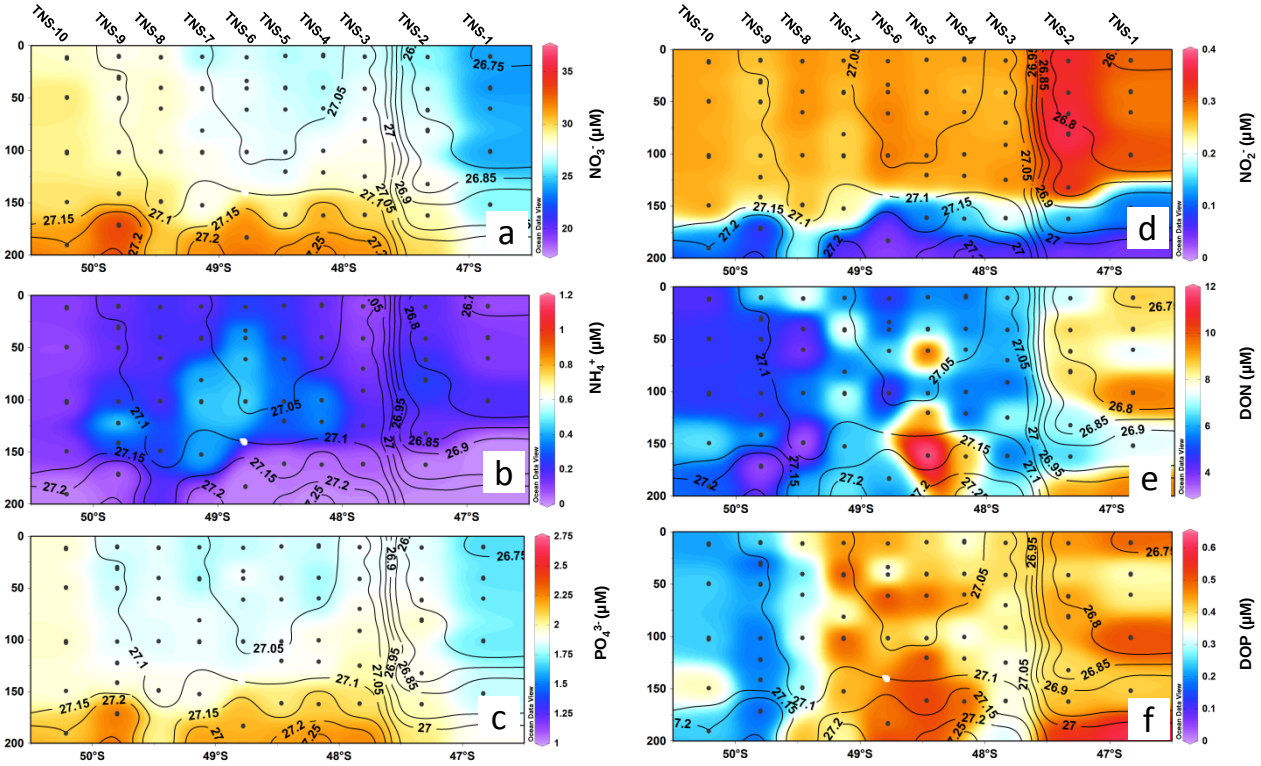
TNS-10
TNS-9
TNS-8
TNS-7
TNS-6
TNS-5
TNS-4
TNS-3
TNS-2
TNS-1
a
b
c
d
e
f
50°S
49°S
48°S
47°S
NO3- (µM)
NH4+ (µM)
PO43- (µM)
NO2- (µM)
DON (µM)
DOP (µM)

Figure 3

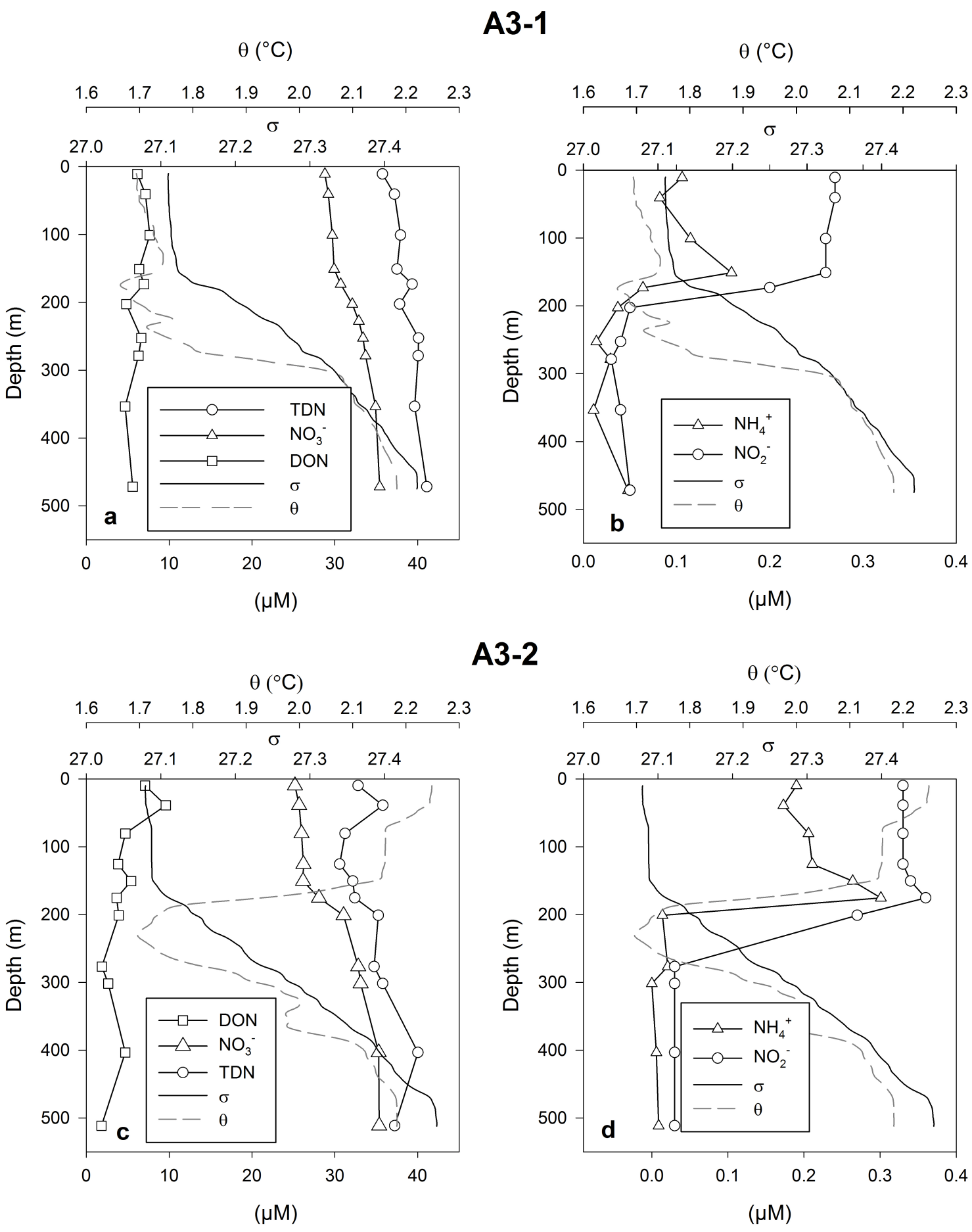
A3-1
θ (°C)
1.6 1.7 1.8 1.9 2.0 2.1 2.2 2.3
σ
27.0 27.1 27.2 27.3 27.4
Depth (m)
0 100 200 300 400 500
TDN
NO3-
DON
σ
θ
a
0 10 20 30 40
(μM)
θ (°C)
1.6 1.7 1.8 1.9 2.0 2.1 2.2 2.3
σ
27.0 27.1 27.2 27.3 27.4
Depth (m)
0 100 200 300 400 500
NH4+
NO2-
σ
θ
b
0.0 0.1 0.2 0.3 0.4
(μM)
A3-2
θ (°C)
1.6 1.7 1.8 1.9 2.0 2.1 2.2 2.3
σ
27.0 27.1 27.2 27.3 27.4
Depth (m)
0 100 200 300 400 500
DON
NO3-
TDN
σ
θ
c
0 10 20 30 40
(μM)
θ (°C)
1.6 1.7 1.8 1.9 2.0 2.1 2.2 2.3
σ
27.0 27.1 27.2 27.3 27.4
Depth (m)
0 100 200 300 400 500
NH4+
NO2-
σ
θ
d
0.0 0.1 0.2 0.3 0.4
(μM)

Figure 4

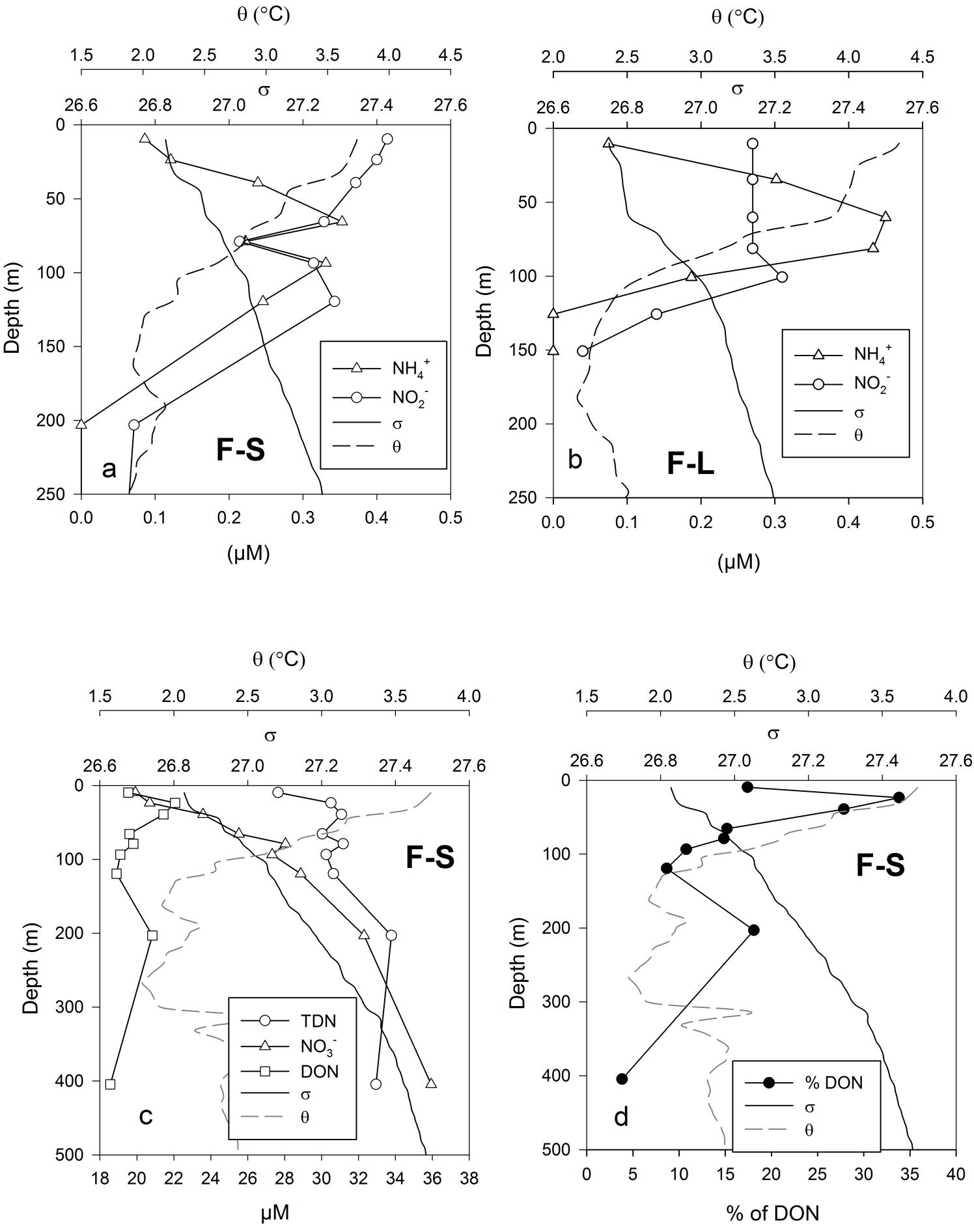
θ (°C)
σ
Depth (m)
(μM)
a
F-S
b
F-L
NH_4^+
NO_2^-
σ
θ
c
F-S
d
F-S
TDN
NO_3^-
DON
% DON
μM
% of DON

Figure 5

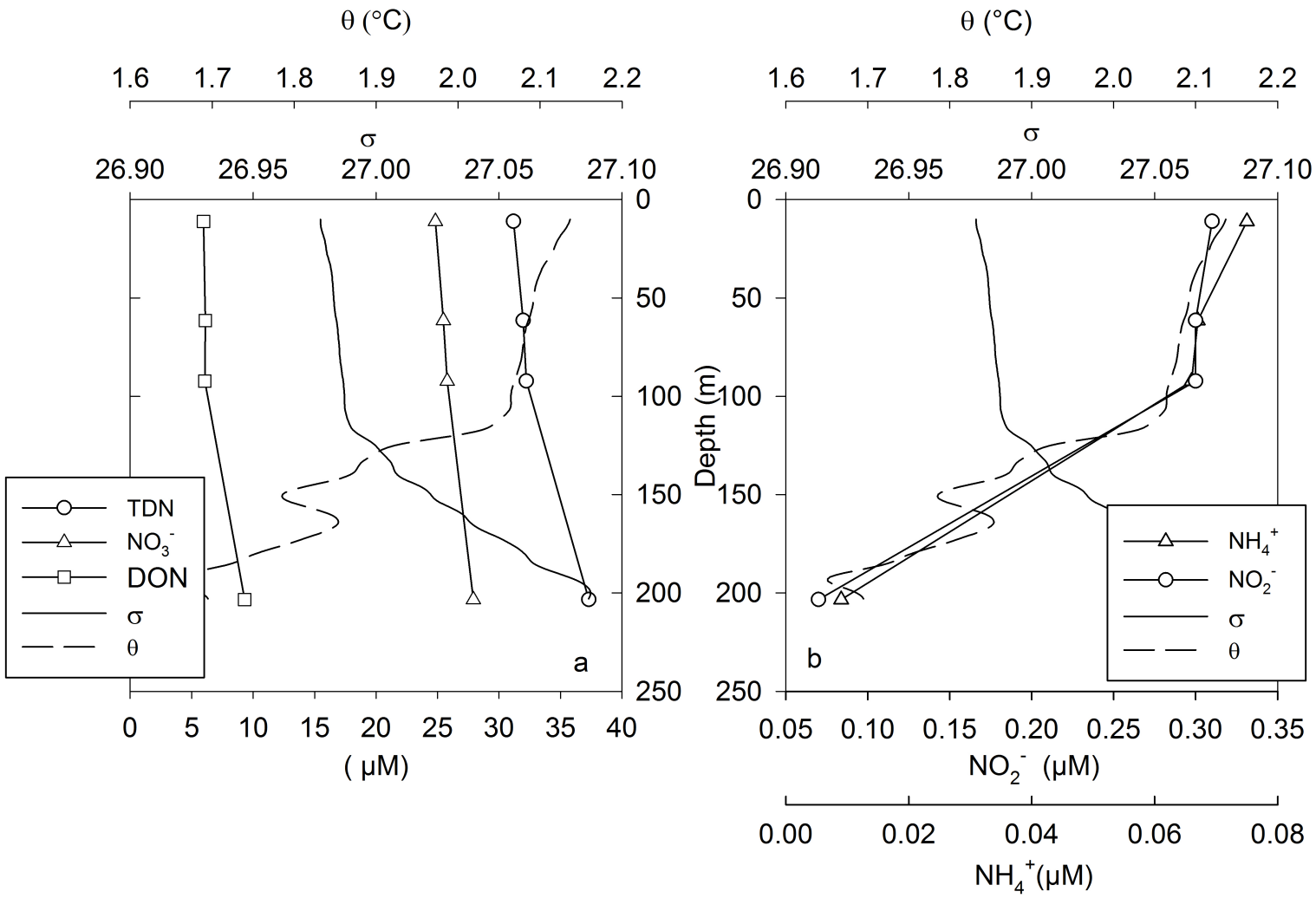
θ (°C)
1.6 1.7 1.8 1.9 2.0 2.1 2.2
σ
26.90 26.95 27.00 27.05 27.10
0 50 100 150 200 250
Depth (m)
TDN
NO3-
DON
σ
θ
a
0 5 10 15 20 25 30 35 40
(μM)
θ (°C)
1.6 1.7 1.8 1.9 2.0 2.1 2.2
σ
26.90 26.95 27.00 27.05 27.10
0 50 100 150 200 250
NH4+
NO2-
σ
θ
b
0.05 0.10 0.15 0.20 0.25 0.30 0.35
NO2- (μM)
0.00 0.02 0.04 0.06 0.08
NH4+(μM)

Figure 6

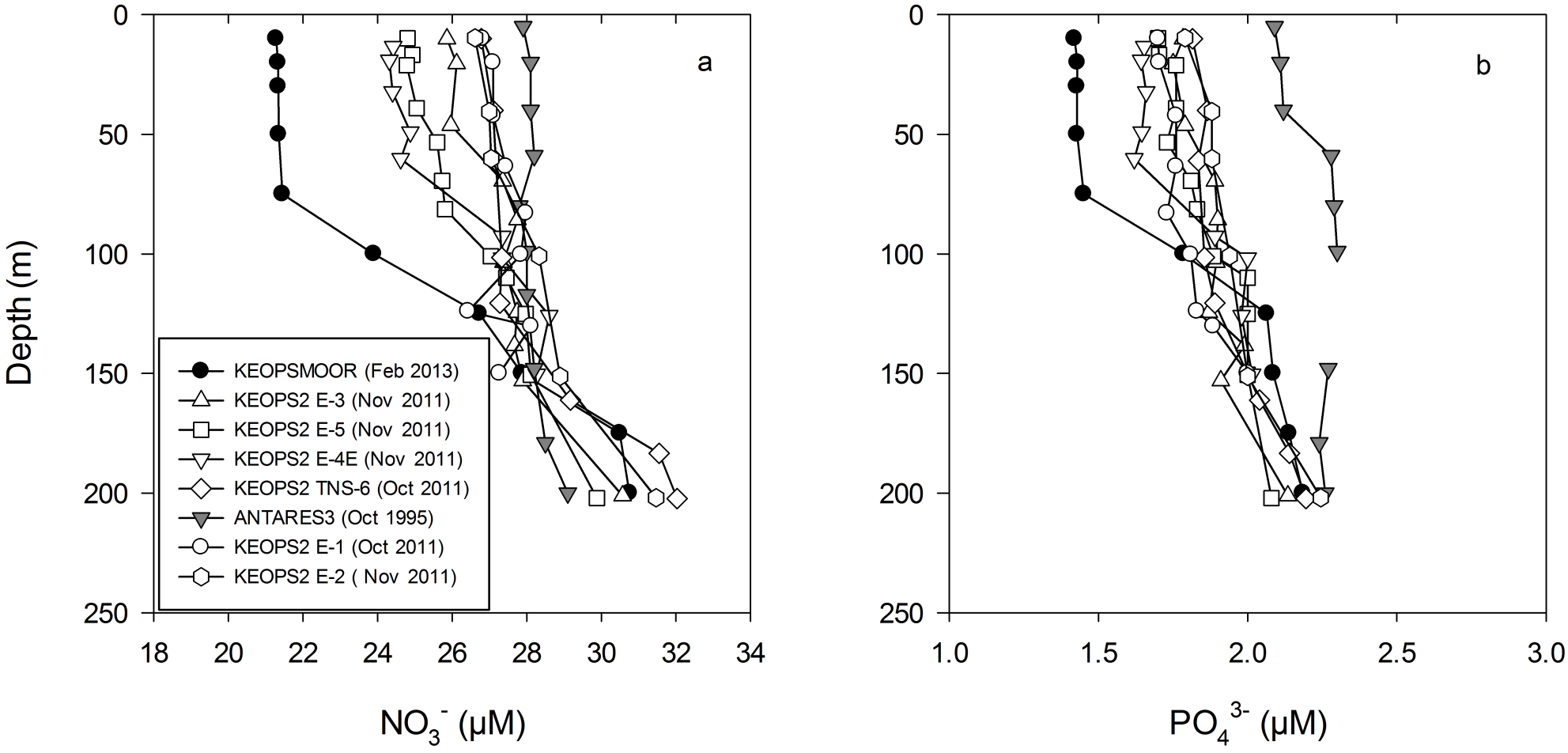
a
b
Depth (m)
0
50
100
150
200
250
18
20
22
24
26
28
30
32
34
1.0
1.5
2.0
2.5
3.0
KEOPSMOOR (Feb 2013)
KEOPS2 E-3 (Nov 2011)
KEOPS2 E-5 (Nov 2011)
KEOPS2 E-4E (Nov 2011)
KEOPS2 TNS-6 (Oct 2011)
ANTARES3 (Oct 1995)
KEOPS2 E-1 (Oct 2011)
KEOPS2 E-2 (Nov 2011)
NO3- (µM)
PO43- (µM)

Figure 7

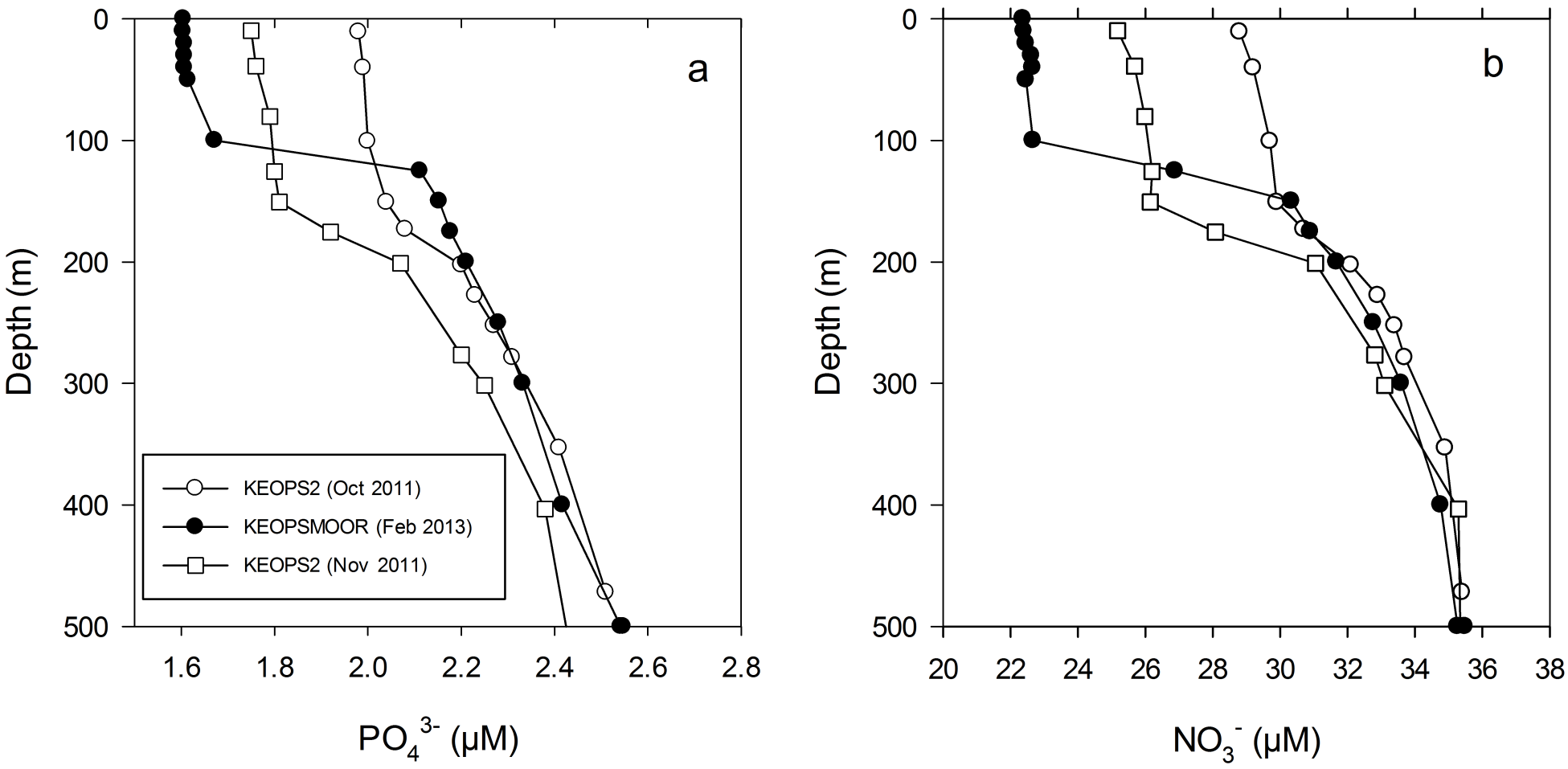
a
b
0
100
200
300
400
500
Depth (m)
1.6
1.8
2.0
2.2
2.4
2.6
2.8
20
22
24
26
28
30
32
34
36
38
KEOPS2 (Oct 2011)
KEOPSMOOR (Feb 2013)
KEOPS2 (Nov 2011)
PO4 3- (µM)
NO3 - (µM)

Figure 8

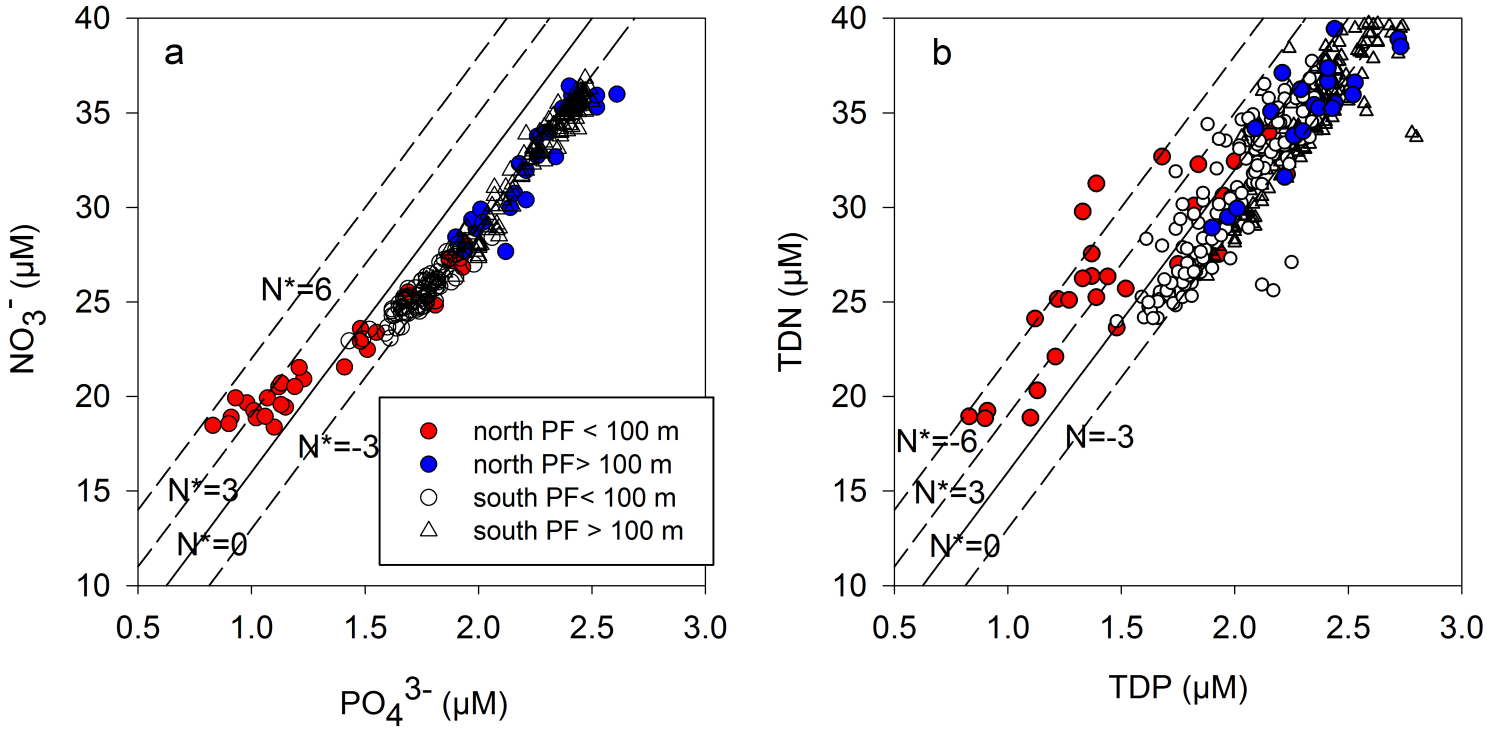
a
b
N*=6
N*=3
N*=0
N*=-3
N=-3
N*=-6
north PF < 100 m
north PF> 100 m
south PF< 100 m
south PF > 100 m
NO3- (µM)
PO43- (µM)
TDN (µM)
TDP (µM)
10
15
20
25
30
35
40
0.5
1.0
1.5
2.0
2.5
3.0

Figure 9

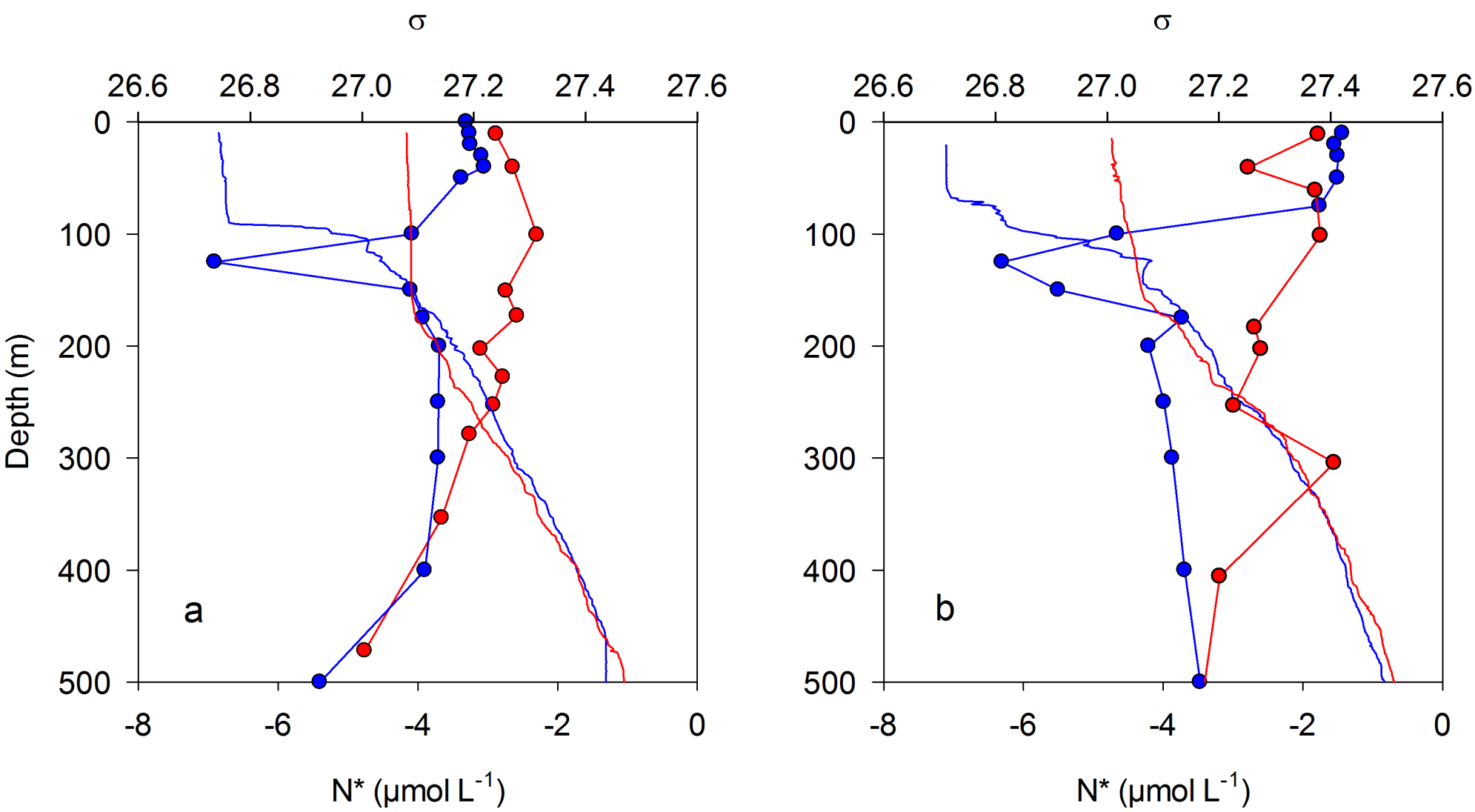
σ
26.6
26.8
27.0
27.2
27.4
27.6
0
100
200
300
400
500
Depth (m)
a
-8
-6
-4
-2
0
N* (µmol L-1)
σ
26.6
26.8
27.0
27.2
27.4
27.6
0
100
200
300
400
500
b
-8
-6
-4
-2
0
N* (µmol L-1)

Figure 10